

Notable Events

The Canterbury, New Zealand
Earthquake Sequence I:
The Mw 7.1 Darfield Earthquake of
3 September 2010 and Aftershock
Sequence

John Ristau

GNS Science, Lower Hutt

New Zealand

Excerpt from the
Summary of the Bulletin of the International Seismological Centre:

Ristau, J., The Canterbury, New Zealand Earthquake Sequence I: The Mw 7.1 Darfield Earthquake of 3 September 2010 and Aftershock Sequence, *Summ. Bull. Internatl. Seismol. Cent.*, July - December 2010, 47(7-12), pp. 48-65, Thatcham, United Kingdom, 2014, doi:10.5281/zenodo.998755.

7

Notable event

7.1 The Canterbury, New Zealand Earthquake Sequence I: The M_w 7.1 Darfield Earthquake of 3 September 2010 and Aftershock Sequence

John Ristau
GNS Science
Lower Hutt
New Zealand



7.1.1 Introduction

On 4 September 2010 at 04:35 NZST (3 September 16:35 UTC) the moment magnitude (M_w) 7.1 Darfield earthquake occurred in the Canterbury region of New Zealand, approximately 10 km southeast of the town of Darfield and 40 km west of Christchurch, New Zealand's second largest city with a population of approximately 377 000 (Figure 7.1). The earthquake was widely felt throughout the South Island and the lower North Island, with over 7300 felt reports received, and caused significant damage in Christchurch, with maximum intensity MM 9 in the epicentral region. Extensive liquefaction and lateral spreading contributed significantly to structural damage observed throughout Christchurch. Through a fortunate combination of strict building codes and the earthquake occurring at night, when the streets were largely deserted, there were no deaths and only two serious injuries reported. Most of the damage, including toppled chimneys and parapets, and failure of gables and frames, was confined to unreinforced brick and masonry structures. Modern buildings and light timber frame structures performed well with little structural damage. The Darfield earthquake was the most damaging earthquake in New Zealand since the 3 February 1931 Hawkes Bay earthquake (M_w 7.4 – 7.6).

The Darfield earthquake was recorded (Figure 7.1) by the national GeoNet broadband and strong-motion networks (Petersen *et al.* 2011) and the regional Canterbury CanNet strong-motion network (Avery *et al.* 2004). Of particular interest is the Canterbury network of nearly 40 seismic instruments that provided dense near-field ground-shaking measurements. Immediately following the Darfield earthquake, GNS Science sent teams of technicians to Christchurch and the Canterbury region to install temporary seismometers and accelerometers to better record the aftershocks. In addition, more than 180 low-cost micro-electro-mechanical accelerometers were deployed to a network of volunteer-owned, internet-connected computers as part of the Quake-Catcher Network (QCN) (Lawrence *et al.* 2014; Cochran *et al.* 2011; Cochran *et al.* 2009). As a result the Darfield earthquake sequence is one of the best recorded earthquake sequences anywhere in the world.

New Zealand straddles the boundary of the Pacific and Australian plates, and the Canterbury region,

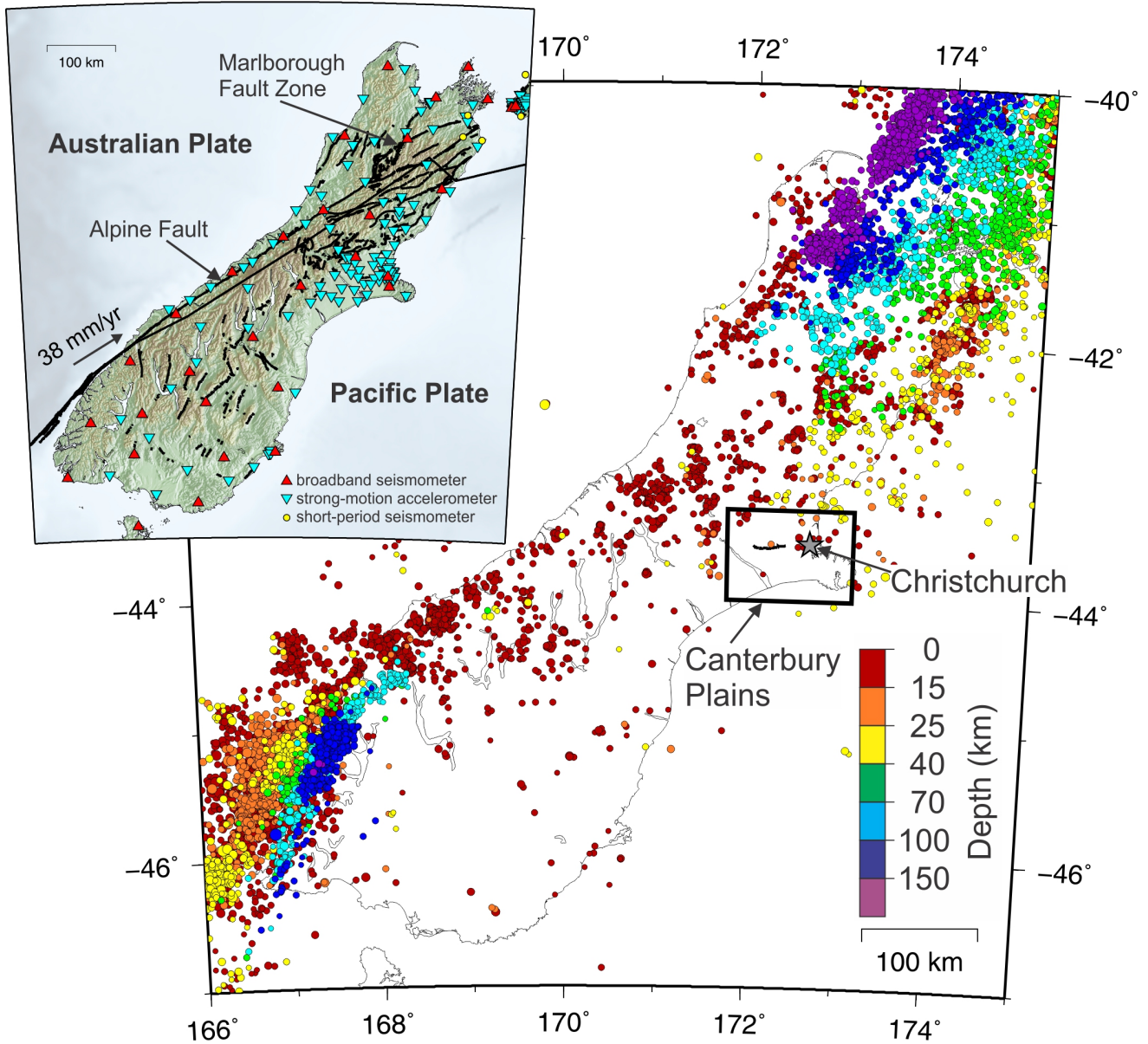


Figure 7.1: Tectonic setting of the South Island of New Zealand, and recorded seismicity ($M \geq 3$) for the 10-year period until 2 September 2010. Major active faults, including the Alpine Fault and Marlborough Fault Zone, are shown by the black lines. Also shown is the seismograph network of broadband seismometers, strong-motion accelerometers, and short-period seismometers operated by GeoNet. Note the low rate of seismicity in the Canterbury Plains region before September 2010.

where the earthquake occurred, is a region of continental convergence about 100 km from the Pacific/Australia plate boundary (Figure 7.1). In the South Island, the Alpine Fault runs along the west coast and accommodates the vast majority of the relative plate motion. Palaeoseismic evidence suggests that the Alpine Fault ruptures in major earthquakes ($M > 7.5$) with recurrence intervals of $\sim 200 - 300$ years, with the most recent event in 1717 (e.g. Cooper and Norris 1990; Yetton *et al.* 1998; Rhoades and Van Dissen 2003; Sutherland *et al.* 2007; Berryman *et al.* 2012). Several $M > 6-7$ earthquakes have occurred in the foothills of the Southern Alps east of the Alpine Fault and west of Christchurch in the past 150 years. These earthquakes include 1888 North Canterbury M_w 7.1 (Cowan 1991), 1929 Arthur's Pass M_w 7.0 (Doser *et al.* 1999), 1994 Arthur's Pass M_w 6.7 (Abercrombie *et al.* 2000) and 1995 Cass M_w 6.2 (Gledhill *et al.* 2000). There are many mapped active faults in the eastern foothills of the Southern Alps (e.g. Stirling *et al.* 2008); however, no active faults had been previously mapped in the Canterbury plains. Dorn *et al.* (2010) carried out high-resolution reflection seismic studies in the western part of the Canterbury Plains. Unfortunately none of the seismic lines crossed the Greendale Fault. The Darfield earthquake demonstrates that the zone of active deformation in the eastern South Island extends beyond the visible range front.

In this paper I present an overview of the Darfield earthquake and its aftershock sequence before the occurrence of the 21 February (UTC) 2011, M_w 6.2 Christchurch earthquake. I will discuss the source properties of the mainshock, characteristics of the aftershock sequence, and review our current understanding of the sequence including stress studies and aftershock forecasts.

7.1.2 Mainshock Source Properties

Before the Darfield earthquake the Canterbury Plains region had a historically low level of seismic activity compared with many other parts of New Zealand (Figure 7.1). In the mid-2000's Canterbury University and GNS Science established CanNet, a network of strong-motion accelerometers around Christchurch and the Canterbury Plains (Avery *et al.* 2004). CanNet was designed to record a future Alpine Fault earthquake; however, it was ideally positioned to record near-field ground motion and directivity effects from the Darfield earthquake. Several stations were located within a few kilometres of the rupture zone (Figure 7.2a). Supplementary instruments were installed (Figure 7.2b) to better record the aftershocks.

The most obvious physical feature of the Darfield earthquake is a 29.5 km long surface rupture on the previously unknown Greendale Fault (Figure 7.3). The Greendale Fault was buried beneath deposits from the last glacial period 18 000 – 20 000 years ago (Forsyth *et al.* 2008). The fault trace cut across mainly well-cultivated, pastoral farmland, which made it quite visible. Relative movement was predominantly right-lateral strike-slip with an average horizontal displacement of ~ 2.5 m, and with maximum displacements of ~ 5 m horizontally and 1.5 m vertically (Quigley *et al.* 2010). However, the Darfield earthquake has been shown to be much more complex than a simple strike-slip event, as was similarly shown for the 2010 M_w 7.0 Haiti earthquake (e.g. Hayes *et al.* 2010).

Teleseismic moment tensor solutions calculated by the USGS (<http://earthquake.usgs.gov/regional/neic/>) and the Global CMT Project (<http://www.globalcmt.org/>) indicated strike-slip faulting consistent with the surface rupture of the Greendale Fault (Figure 7.2c; Table 7.1). In contrast, the GeoNet regional moment tensor solution and GeoNet first-motion solution indicated reverse faulting on either a shallow

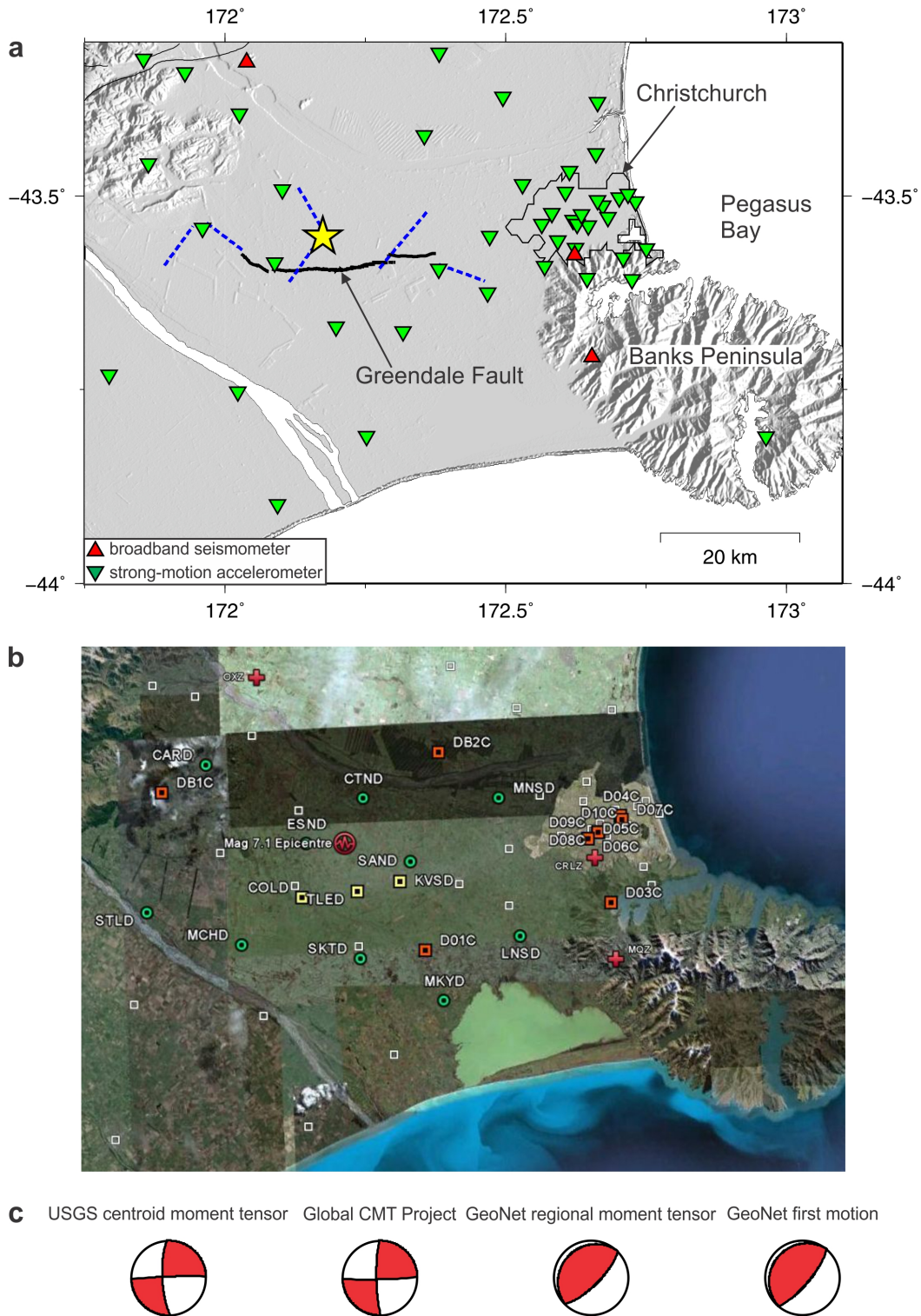


Figure 7.2: a) Seismograph network in the Canterbury region at the time of the M_w 7.1 Darfield earthquake (yellow star). Inferred subsurface faults (dashed lines) are those of Beavan et al. (2012), Elliot et al. (2012) and Atzori et al. (2012). Broadband seismometers are indicated by red triangles, and Canterbury University (CanNet) strong-motion accelerometers by inverted green triangles. (b) Temporary short-period seismometer (green circles) and accelerometer (yellow and orange squares) networks installed immediately following the Darfield earthquake. (c) Focal mechanisms for the Darfield earthquake from the USGS centroid moment tensor, Global CMT Project, GeoNet regional moment tensor, and GeoNet first-motion analyses.

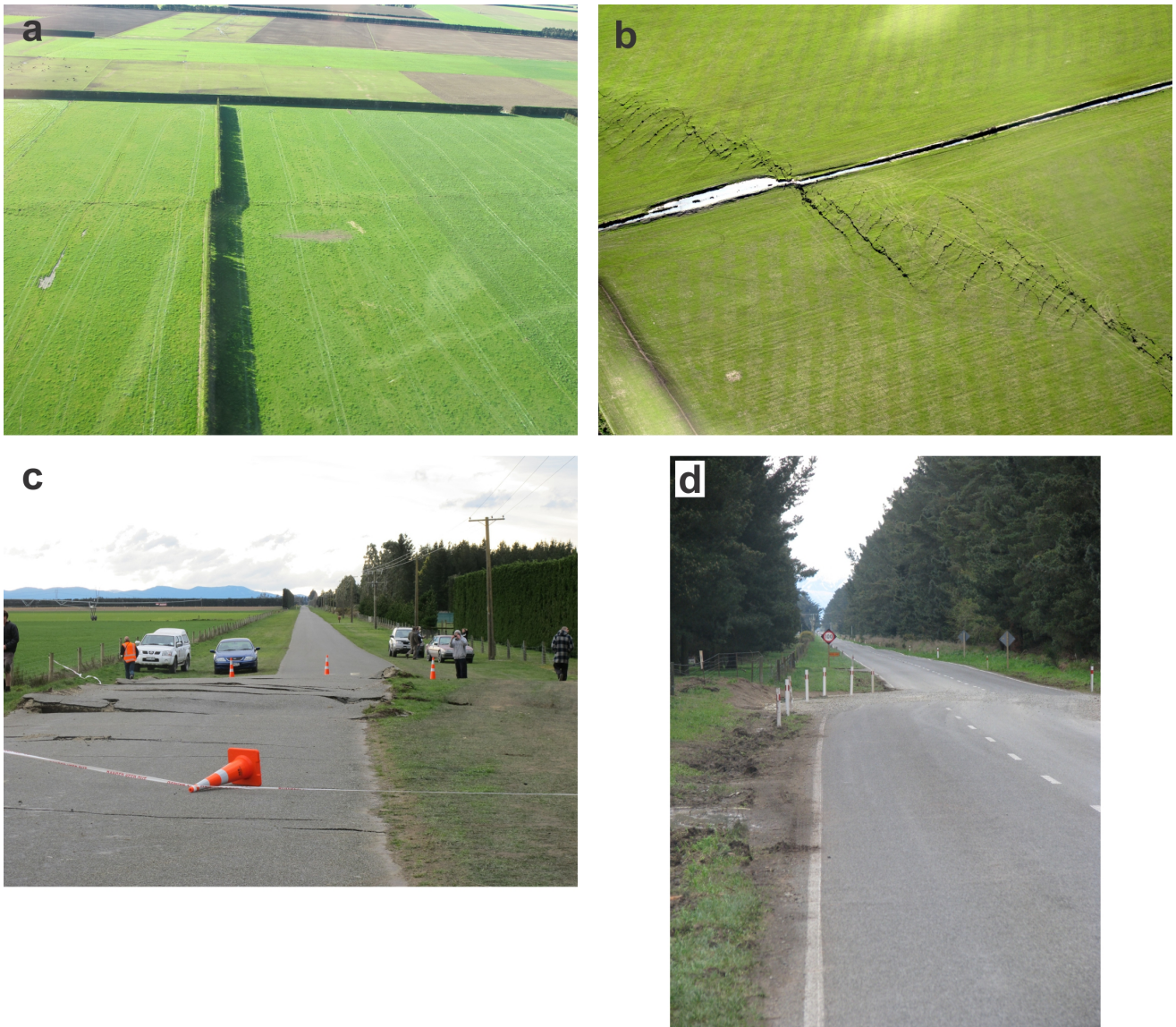


Figure 7.3: Examples of surface rupture and displacement along the Greendale Fault. (a) Greendale Fault trace, photographer David Barrell, copyright GNS Science/EQC, VML ID 112421. (b) Greendale Fault trace, photographer Richard Jongens, copyright GNS Science/EQC, VML ID 114908. (c) Highfield Road surface rupture and displacement, photographer David Barrell, copyright GNS Science/EQC, VML ID 118544. (d) Road displacement, photographer John Begg, copyright GNS Science/EQC, VML ID 99707.

NW-dipping plane or a steep SE-dipping plane (Figure 7.2c; Table 7.1). As a result of the high density of strong-motion stations in the vicinity of the mainshock, the hypocentre estimate was well constrained about 4 ± 0.5 km north of the surface trace of the Greendale Fault (Gledhill *et al.* 2011). Due to the well-constrained hypocentre, with an estimated depth of about 11 km, the discrepancy between the hypocentre location and the trace of the Greendale Fault cannot be explained by the location uncertainty. A shallow-dipping fault plane could account for the discrepancy, but there should be near co-incidence of the epicentre with the trace of the Greendale Fault for any near-vertical strike-slip mechanism as indicated in the global moment tensor solutions.

Table 7.1: Source parameters for the Darfield earthquake.

Agency/Type	strike/dip/rake	strike/dip/rake	M_o (Nm)	M_w	Depth (km)
USGS centroid moment tensor	268/87/-166	178/77/-3	3.50E+19	7.0	10
Global CMT Project	179/82/3	88/87/172	3.49E+19	7.0	12
GeoNet regional moment tensor	45/73/90	226/17/91	6.10E+19	7.1	8
GeoNet first motion	40/75/90	220/15/90	n/a	n/a	n/a

The teleseismic moment tensor methods may not be able to resolve the distinct mechanisms but instead provide an average over the whole event, which is dominated in this case by slip along the Greendale Fault. The regional moment tensor solution and the first-motion solution used near-source or regional data, making them more sensitive to small-scale features. As a result the GeoNet solutions model the nature of the initial reverse-faulting rupture.

More evidence of a complex rupture comes from strong-motion accelerometer data, which suggest that there were at least three distinct fault ruptures in the sequence (Figure 7.4; Holden and Beavan 2012). The kinematic source model is consistent with an initial rupture on a steeply dipping, blind reverse fault (Charing Cross Fault) with a rupture duration of 3 – 6 s and M_w 6.2. The initial rupture then triggered the Greendale Fault with a rupture duration of 8 – 18 s and a maximum displacement of 5 m at the surface. This Greendale Fault rupture was equivalent to a M_w 6.8 earthquake, making it the largest event of the sequence. After 17 s, a reverse fault at the western end of the Greendale Fault near Hororata was triggered with a M_w 5.7 event. The overall moment release in the kinematic model is equivalent to a M_w 6.9 earthquake.

Geodetic studies of the mainshock using combinations of GPS and InSAR data have been carried out by Beavan *et al.* (2012), Atzori *et al.* (2012) and Elliot *et al.* (2012). All of the geodetic models require multiple fault segments to be active during the earthquake. Beavan *et al.* (2012) used seven individual segments to model the rupture zone (Figure 7.5). The Beavan *et al.* (2012) model requires a steep SE-dipping reverse fault several kilometres north of the Greendale Fault as the initial M_w 6.4 rupture. This is consistent with the hypocentre location, GeoNet focal mechanisms and kinematic results. The M_w 6.8 main rupture was along the Greendale Fault with an average slip of 2.8 m. Several other reverse faulting and strike-slip faulting segments were also active, giving an equivalent M_w 7.1 for the entire sequence. The Elliot *et al.* (2012) and Atzori *et al.* (2012) geodetic models also require multiple ruptures with initial reverse faulting several kilometres to the north of the Greendale Fault.

Peak ground accelerations (PGA) in the Canterbury Plains and Christchurch are shown in Figure 7.6. The largest recorded PGA's were > 1.2 g near the Greendale Fault and to the east of the Greendale

West

East

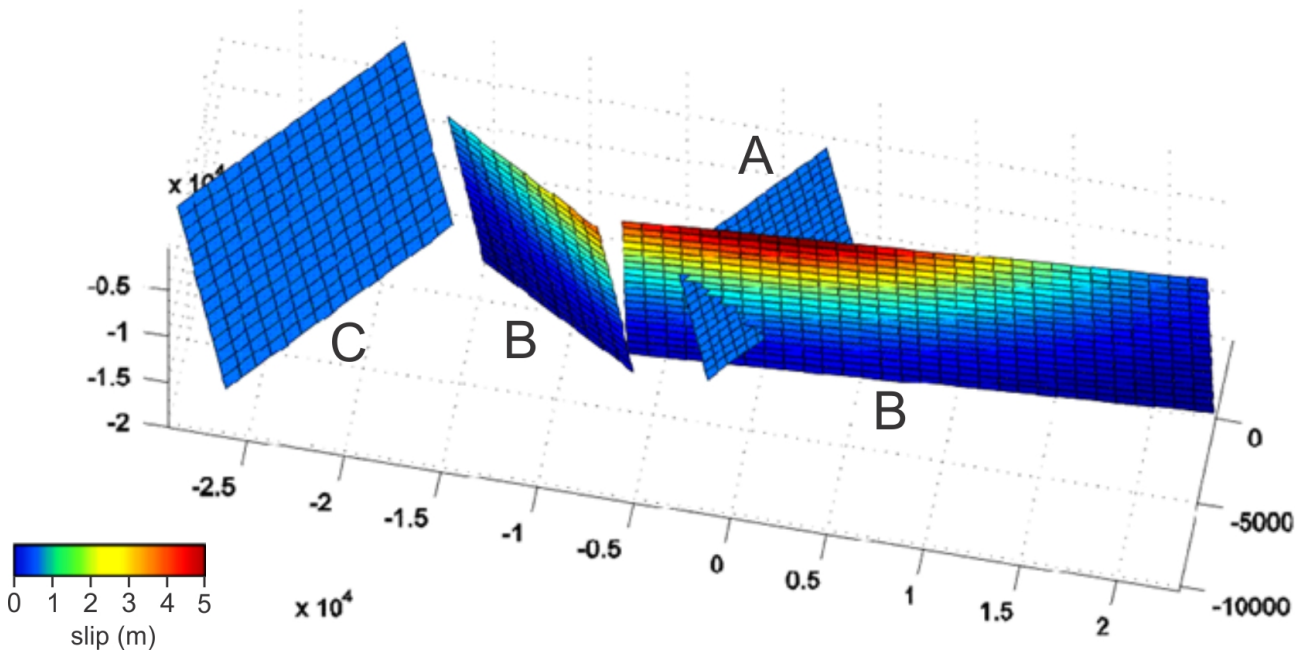


Figure 7.4: Kinematic source model of the Darfield earthquake showing three distinct fault ruptures. A is the Charing Cross reverse fault where the rupture initiated; B is the Greendale Fault; and C is the reverse fault at the western end of the rupture zone.

Fault. In Christchurch the observed PGA's were lower, typically $\sim 0.2 - 0.3$ g, although some large horizontal PGA's were recorded SE of the city centre (Figure 7.6). These ground motions were sufficient to generate extensive regions of liquefaction in many areas of Christchurch.

The crustal structure in the Canterbury region is dominated by the Hikurangi Plateau – a large igneous province that was subducted ~ 100 million years ago. The Hikurangi Plateau is extremely strong and remains attached to the crust, capped by schist and greywackes containing east-west Cretaceous faults (Reyners *et al.* 2013). As a result of the strength of the crust, the radiated energy (E_S) and apparent stress (τ_a) for the Darfield earthquake were very large. The apparent stress is defined as the product of the rigidity and the E_S per unit moment, which means the apparent stress is greater with stronger crust and larger E_S . Fry and Gerstenberger (2011) calculated τ_a of ~ 16 MPa for Darfield, which is significantly greater than global averages for τ_a (e.g. Choy *et al.* 2001; Atkinson and Boore 2006)

The Darfield earthquake involved reactivation of east-west Cretaceous faults that are favourably oriented in the regional stress field. In the region of the Greendale Fault, Reyners *et al.* (2013) found unusually low P- to S-wave velocity ratios of 1.60 compared to 1.71 before the Darfield earthquake. Reyners *et al.* (2013) interpreted this reduced velocity ratio as the signature that the greywackes had been weakened by the rupture front producing widespread cracking around the fault zone. Sibson *et al.* (2011) concluded that the fault system appears to be controlled by the orientation of the tectonic stress field in the upper crust rather than conforming to local plate boundary kinematics. Furthermore, based on anisotropic seismic tomography, Fry *et al.* (2014) suggest that the crust underlying the Canterbury Plains is dominated by faulting parallel to the Greendale Fault. Therefore, the Darfield earthquake can be regarded as an intraplate event, remote from the main Alpine-Marlborough fault system that defines

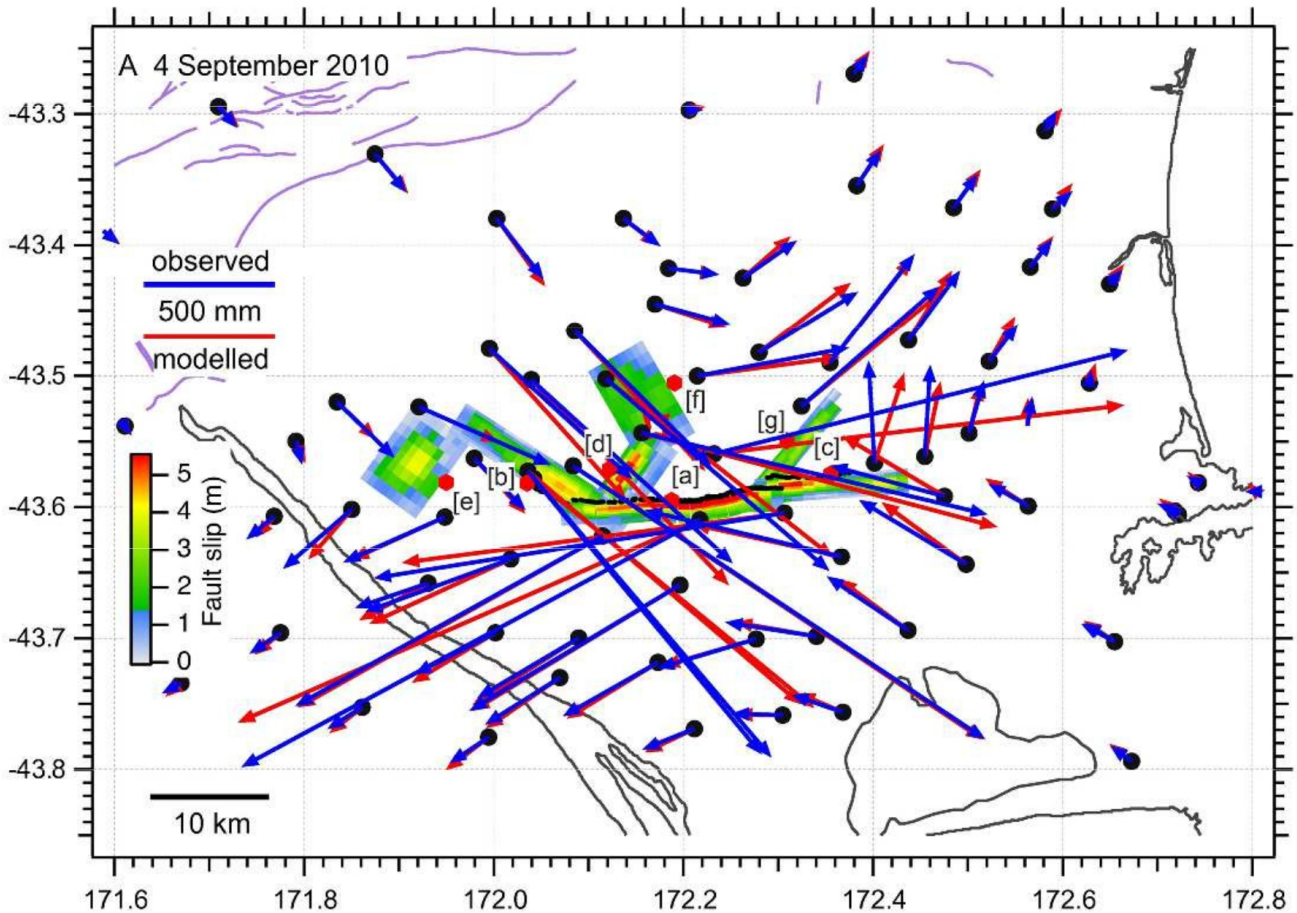


Figure 7.5: Observed (blue) and modelled (red) displacements at GPS sites, and the slip model derived from GPS and DInSAR for the Darfield earthquake. Red dots with adjacent letters in square brackets (e.g. [a]) are located where the centres of the fault segments would outcrop if extended to the surface (from Beavan *et al.* 2012).

the Pacific/Australian plate boundary.

7.1.3 Aftershock Sequence

A well-recorded aftershock sequence followed the Darfield earthquake with over 5000 located events with $M_L \geq 1.7$, and 15 with $M_L \geq 5.0$, in the period from 3 September 2010 – 21 February 2011 (Figure 7.7a). More than 4000 of the aftershocks were relocated using a double-difference tomography method (Bannister *et al.* 2011). The resulting aftershock distribution shows a NNW-SSE oriented trend of aftershocks off the main alignment, consistent with the initial rupture being located to the north of the Greendale Fault. Another cluster of aftershocks is present at the western end of the rupture zone, corresponding to one of the fault segments in the geodetic model. There is also a NE-SW line of aftershocks from the eastern end of the fault zone leading into Christchurch.

Focal mechanisms from 153 regional moment tensor solutions show a variety of faulting styles, providing additional evidence for the complex nature of the rupture process (Figure 7.7b). The initial rupture was a reverse faulting mechanism as discussed earlier. Other focal mechanisms in the immediate area of the initial rupture are for a mixture of reverse and strike-slip faulting. At the western end of the fault

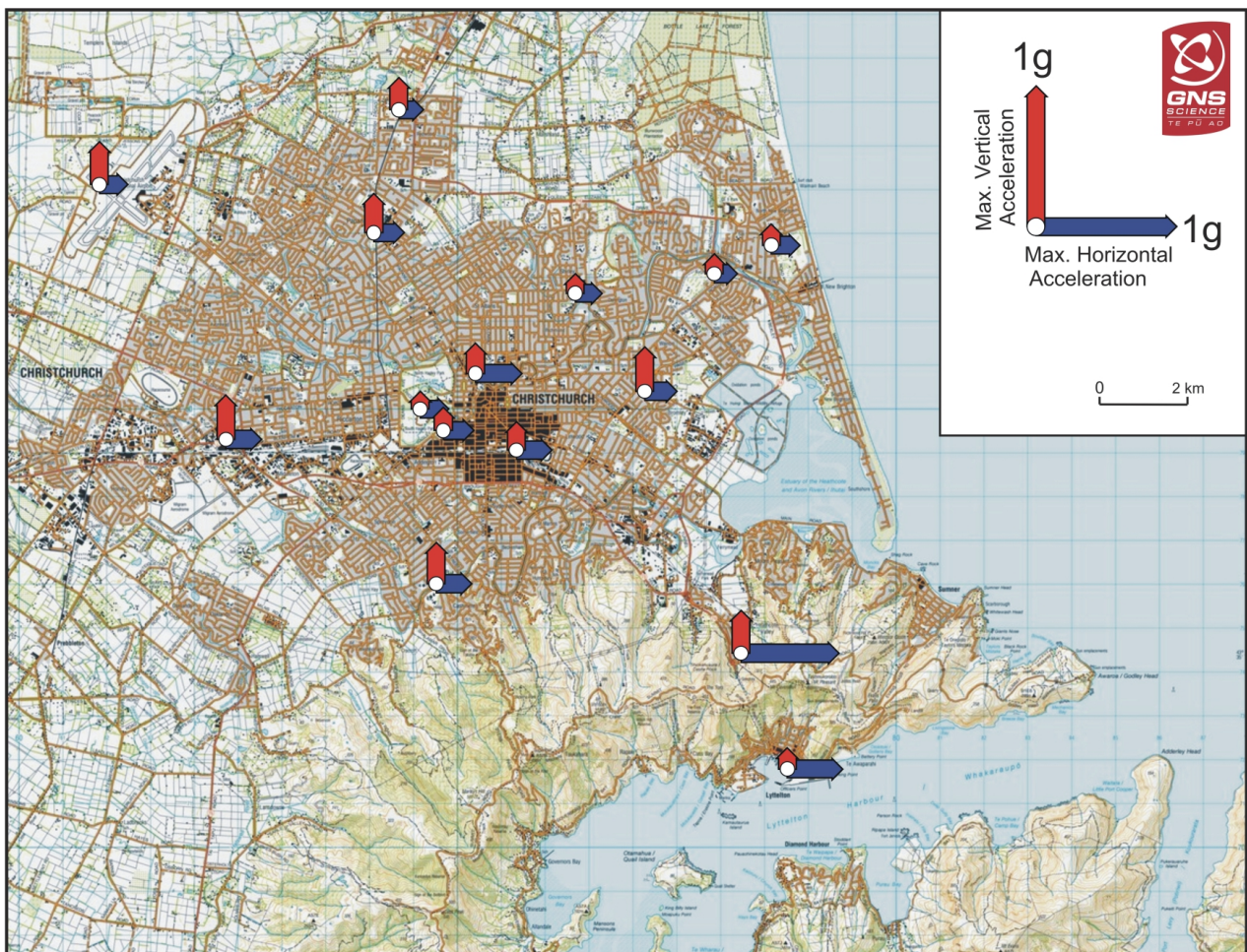
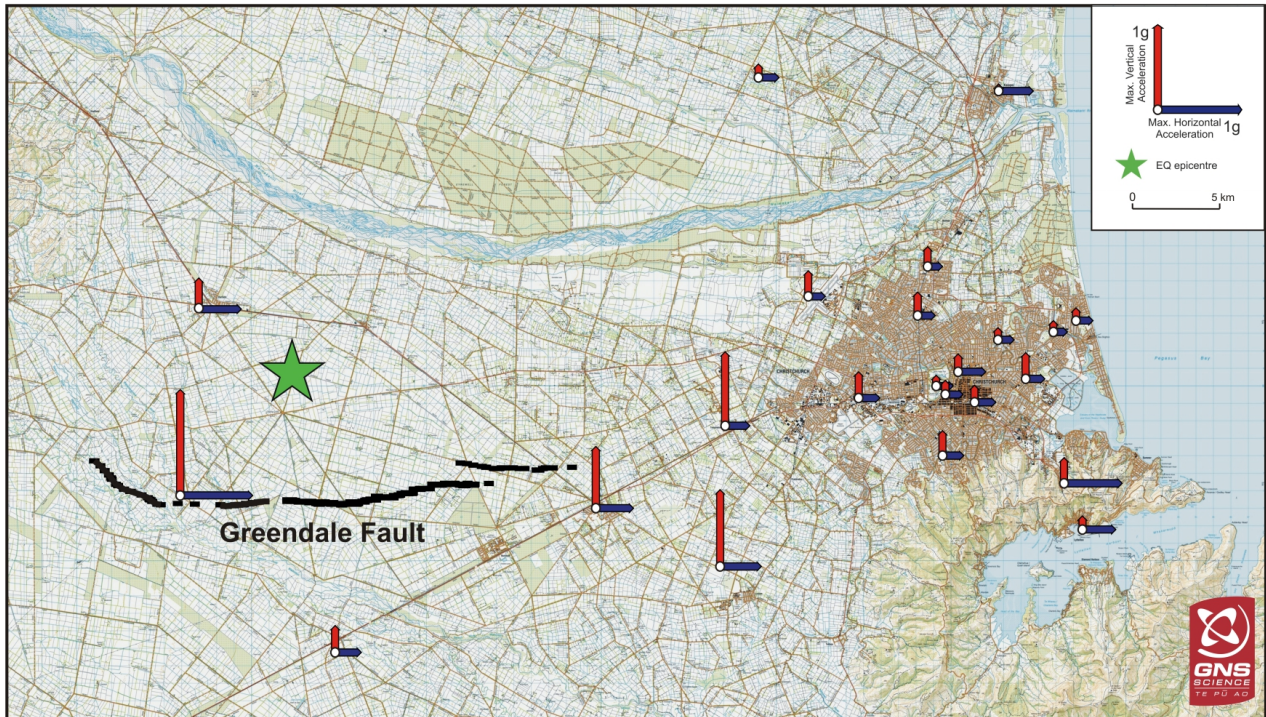


Figure 7.6: Peak ground accelerations from the Darfield earthquake in the Canterbury Plains and Christchurch. The largest observed PGA's were greater than 1.2 g near the Greendale Fault (black line). In Christchurch PGA's were typically $\sim 0.2 - 0.3$ g, although some larger horizontal accelerations were recorded SE of the city.

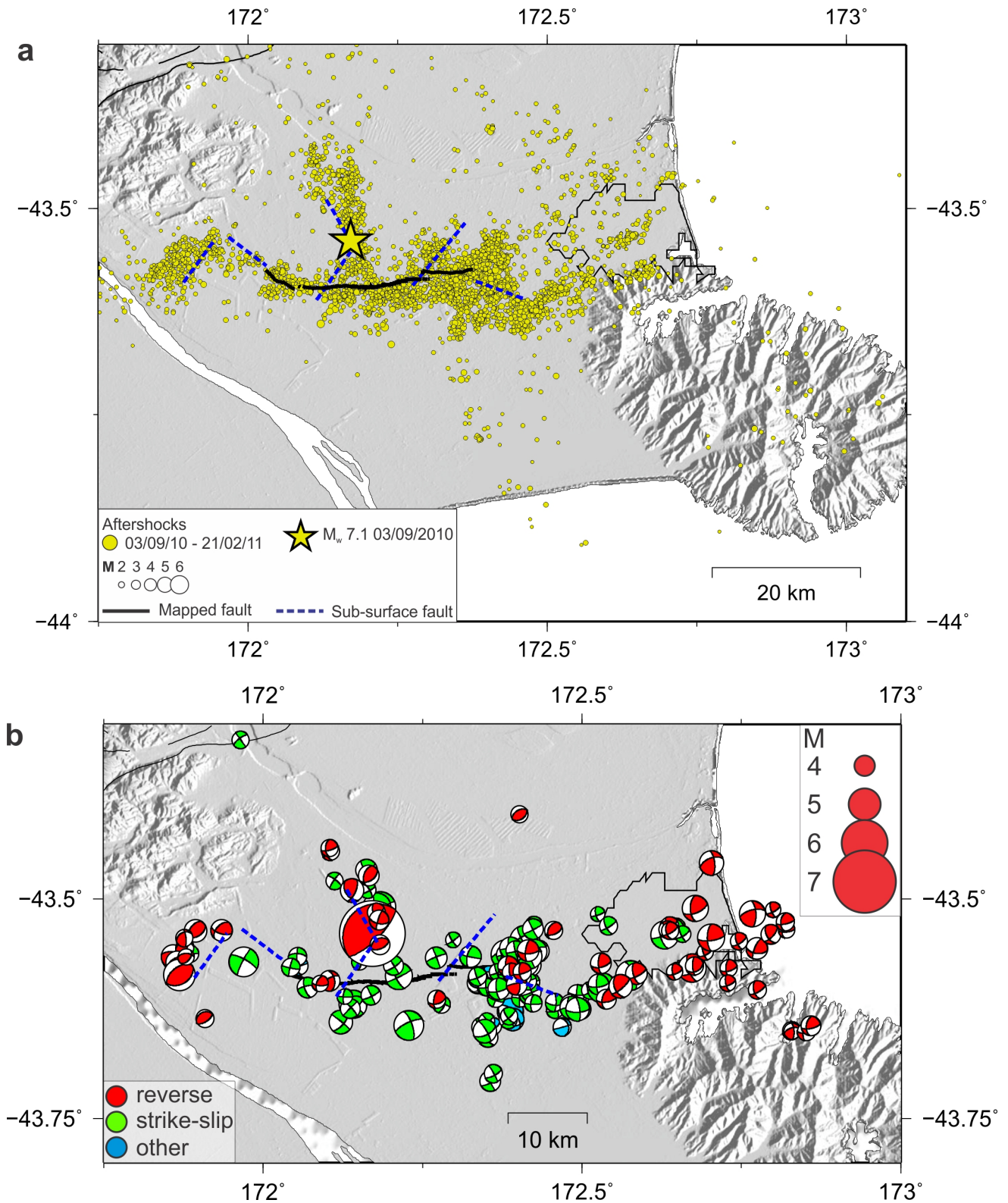


Figure 7.7: (a) Relocated aftershocks for the period 3 September 2010 – 21 February 2011. The solid black line is the Greendale Fault and the dashed blue lines are inferred subsurface faults. (b) Focal mechanisms derived from 153 regional moment tensor solutions for the period 3 September 2010 – 21 February 2011. Strike-slip faulting is dominant along the Greendale Fault. The focal mechanisms are for predominantly reverse faulting at the western end of the rupture zone and around Christchurch.

zone the mechanisms are predominantly for reverse faulting, consistent with the geodetic model of the main rupture, which includes a reverse faulting segment at the western end of the rupture zone. East of the main rupture zone, leading into Christchurch, focal mechanisms are mainly for reverse faulting or oblique-reverse faulting.

The aftershock locations mostly coincide with the Greendale Fault trace and the location of inferred subsurface faults (Figure 7.7a,b). However, at the eastern end of the Greendale Fault there is a NE-SW trend of aftershocks that are not associated with any known subsurface fault, and this is particularly noticeable in the plot of focal mechanisms (Figure 7.7b). There is also a NE-SW trend of aftershocks between the Greendale Fault and Christchurch that is also not associated with any known subsurface fault, and in this region the focal mechanisms change from mainly strike-slip faulting in the west to oblique-reverse faulting closer to Christchurch.

On 26 December 2010 NZST (25 December 2010 UTC) a cluster of very shallow aftershocks occurred near the Christchurch city centre. The largest, M_w 4.7, occurred at 12:30 NZST when the city centre was highly populated (Ristau 2011). These aftershocks were widely felt and the M_w 4.7 event caused damage to brick and masonry structures already weakened in the city centre. Three moment tensor solutions were calculated for events in this series of aftershocks, all with strike-slip mechanisms. Ristau (2011) also calculated 16 first-motion focal mechanisms for events in this series, including the three events for which moment tensor solutions had been calculated, and although the first-motion mechanisms were for mainly reverse faulting, the P-axis orientation is consistent with those in the moment tensor solutions.

7.1.4 Stress Studies and Aftershock Forecasts

Steady *et al.* (2014) studied stress triggering during the Canterbury earthquake sequence by comparing maps of Coulomb stress changes with the location of future events. They investigated whether later large aftershocks were consistent with stress triggering, and whether a simple stress map produced shortly after the Darfield earthquake would have accurately indicated the regions where subsequent activity occurred. Steady *et al.* (2014) found that all aftershocks with $M > 5.5$ occurred in positive stress areas computed using a slip model for Darfield that was available within 10 days of its occurrence. They also found a stress increase of up to 0.24 MPa on the Porter's Pass fault – an active fault ~ 80 km NW of Christchurch capable of generating a M_w 7.5 earthquake. Figure 7.8 shows modelled principal stress (σ_1) deflections in the region of the Darfield rupture zone, with the thick red line indicating the compressional direction of the regional stress field (S. Ellis, pers. comm.). Along the Greendale Fault σ_1 is rotated up to 15° counterclockwise, while at the eastern end of the rupture zone and north of the Greendale Fault σ_1 is rotated up to 15° clockwise.

During the Canterbury earthquake sequence GNS Science provided regular aftershock probability forecasts (e.g. Gerstenberger *et al.* 2014). As the sequence progressed the forecasts varied between daily, weekly and monthly forecasts as required. Figure 7.9 and Table 7.2 show various forecasts for M 4.0 – 4.9 and $M \geq 5.0$. During the first day the observed number of aftershocks in the M 4.0 – 4.9 and $M \geq 5.0$ ranges were higher than the model predicted. After the first day the observed number of aftershocks fell within the ranges predicted by the models.

Table 7.3 shows 1-week, 1-month and 1-year aftershock probabilities calculated on 13 October 2010 for M

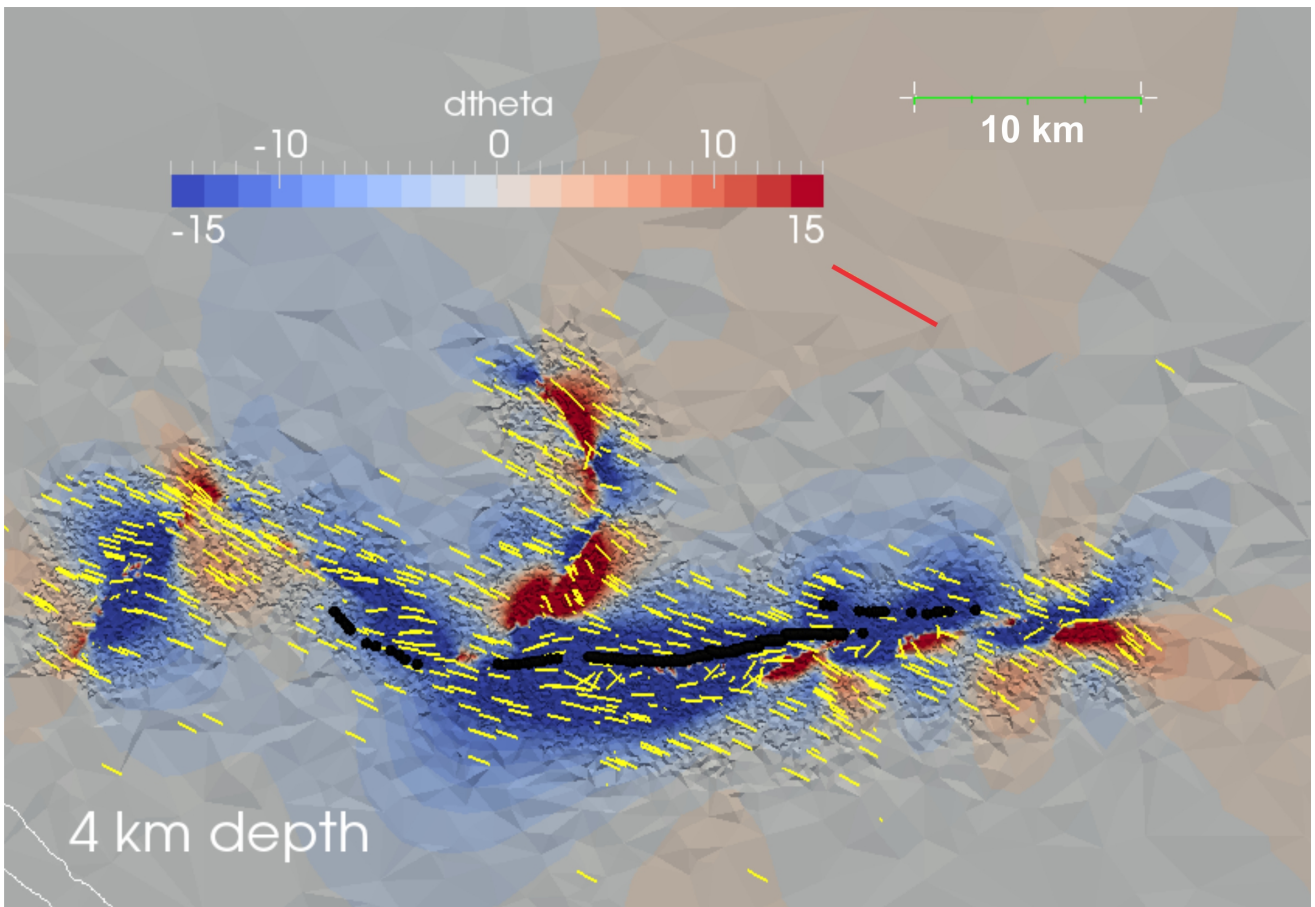


Figure 7.8: Principal stress (σ_1) deflections in the region of the Darfield rupture zone. The thick red line is the compressive direction of the regional stress field, $d\theta$ is the contoured change in degrees from the regional stress field, and the yellow lines are the calculated values. Along the Greendale fault there is a counterclockwise rotation in σ_1 with respect to the regional stress field. At the eastern end of the rupture zone and north of the Greendale fault there is a clockwise rotation of σ_1 .

Table 7.2: Expected and observed numbers of aftershocks.

Date (NZST)	Expected number of aftershocks M 4.0 - 4.9	Observed	Expected number of aftershocks $M \geq 5.0$	Observed
4 September 2010 - M_w 7.1	43 - 73	114	2 - 12	18
5 September 2010	11 - 29	19	0 - 5	1
6 - 12 September 2010	28 - 53	37	1 - 9	4
13 - 19 September 2010	8 - 23	20	0 - 5	0
20 - 26 September 2010	4 - 16	9	0 - 3	0
27 September - 3 October 2010	2 - 13	3	0 - 3	0
4 - 31 October 2010	10 - 26	15	0 - 4	3
1 - 28 November 2010	5 - 17	11	0 - 4	0
29 November - 26 December 2010	3 - 13	3	0 - 3	0
27 December 2010 - 23 January 2011	2 - 11	7	0 - 3	1
24 January - 20 February 2011	1 - 9	5	0 - 2	0
21 - 22 February 2011	0 - 2	0	0 - 1	1

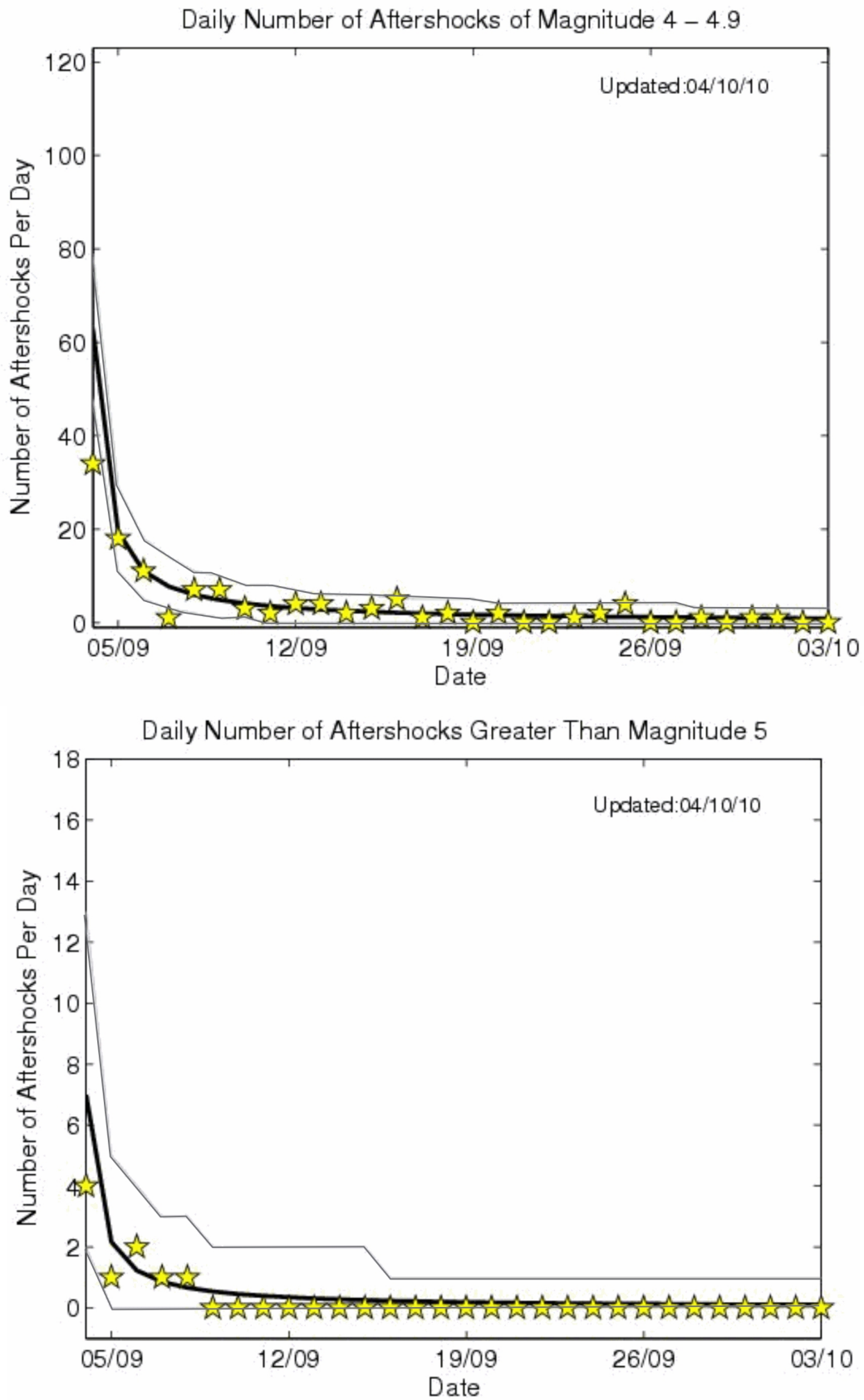


Figure 7.9: Aftershock probability forecasts for M 4.0 – 4.9 (top) and $M \geq 5.0$. The black line is the number of aftershocks predicted by the model, grey lines are the confidence limits, and the yellow stars are the observed number of aftershocks. The number of aftershocks predicted by the model fits well with the observed number of aftershocks.

5.0 – 5.9, M 6.0 – 6.9 and M 7.0+, valid for the entire Canterbury Plains region, including Christchurch. It is important to note that these probabilities were calculated using an incomplete catalogue as only about half the aftershocks had been located at the time, including only about one-half to one-third of those of $M \geq 5$ (A. Christophersen, pers. comm.). Table 7.3 gives a probability 28 – 46% for a M 6.0 – 6.9 aftershock within one year. By 27 January 2011 the one-year probability of a M 6.0 – 6.9 aftershock had dropped by about half to 15 – 28%, and the one-month probability was 2.6 – 4.8%. At this point a 21 February 2011 (UTC) M_w 6.2 Christchurch earthquake could be seen as a lower probability event, although the computed probabilities may have been significantly higher with a more complete dataset.

Table 7.3: *Aftershock probabilities for given magnitude ranges.*

Date	M 5.0 - 5.9			M 6.0 - 6.9			M 7.0+		
	1-week	1-month	1-year	1-week	1-month	1-year	1-week	1-month	1-year
13 Oct 2010	19-35%	51-81%	93-100%	2.5-4.2%	8-14%	28-46%	0.4-0.5%	1.2-1.7%	4.6-6.6%
27 Jan 2011	19-39%	74-96%	74-96%	0.7-1.2%	2.6-4.8%	15-28%	0.09-0.14%	0.37-0.55%	2.3-3.6%

7.1.5 Discussion

In this paper I have summarised some of the major findings from the M_w 7.1 Darfield earthquake and its aftershock sequence. The evidence has shown that the Darfield earthquake initiated several kilometres north of the Greendale Fault and the rupture involved multiple fault segments. Geodetic and kinematic studies have shown that the Darfield sequence began as a steeply dipping reverse-faulting event, continued by triggering the Greendale Fault as a right-lateral strike-slip event that accommodated the majority of the moment release, and also involved several other reverse faulting events at either end of the Greendale Fault.

The located aftershocks show a NNW-SSE oriented trend off the main alignment, consistent with the hypocentre being located north of the Greendale Fault. Regional moment tensor solutions indicate the complexity of the rupture zone, with mainly strike-slip faulting in the vicinity of the Greendale Fault, and with reverse faulting dominant at the western and eastern ends of the Greendale Fault and through to Christchurch.

Stress modelling using a model available within 10 days of the mainshock showed that all the $M > 5.5$ aftershocks occurred in areas of increased stress. Aftershock probability forecasts accurately modelled the number of M 4.0 – 4.9 and $M \geq 5.0$ aftershocks from 3 September 2010 – 21 February 2011. Early in the aftershock sequence (13 October 2011) the one-year probability of a M 6.0 – 6.9 aftershock was 28 – 46%, and on 27 January 2011 it was 15 – 28%. Typically there should have been a large aftershock about one magnitude unit less than that for the mainshock, but none such had occurred early in the sequence.

7.1.6 Conclusions

The M_w 7.1 Darfield earthquake was the most damaging earthquake in New Zealand since the 3 February 1931 Hawkes Bay earthquake (M_w 7.4 – 7.6). As a result of the network of strong-motion instruments operating in the Canterbury Plains and Christchurch before the mainshock, the Darfield earthquake is

one of the best recorded major earthquakes anywhere in the world. The near-field strong-motion dataset will be invaluable to future seismic hazard and engineering studies in New Zealand and elsewhere. The complexity of the main rupture further supports the idea that major earthquakes involve multiple rupture segments such as observed for the 2010 Haiti M_w 7.0 (Hayes *et al.* 2010), 2008 Wenchuan M_w 7.9 (Zhang and Ge 2010) and 2002 Denali M_w 7.9 (Eberhart-Phillips *et al.* 2003) events. On 21 February 2011 (UTC) a M_w 6.2 aftershock occurred beneath the outer suburbs of Christchurch and resulted in 185 fatalities and widespread building damage.

7.1.7 Acknowledgements

This paper would not have been possible without many valuable discussions and much input from Stephen Bannister, John Beavan, Anne-Marie Christophersen, Susan Ellis, Bill Fry, Matt Gerstenberger, Caroline Holden, Anna Kaiser, Martin Reyners, Rick Sibson, Sandy Steacy and Charles Williams. Many of the figures were created using Generic Mapping Tools (GMT) (Wessel and Smith 1991). Photographic images are reproduced with the kind permission of GNS Science/EQC.

7.1.8 References

- Abercrombie, R.E., T.H. Webb, R. Robinson, P.G. McGinty, J. Mori, and R.J. Beavan (2000). The enigma of the Arthur's Pass, New Zealand earthquake 1. Reconciling a variety of data for an unusual earthquake sequence. *Journal of Geophysical Research* 105, 16119-16137.
- Atkinson, G.M., and D.M. Boore (2006). Earthquake ground-motion prediction equations for eastern North America. *Bulletin of the Seismological Society of America* 96, 2181-2205.
- Atzori, S., C. Tolomei, A. Antonioli, J. Merryman, S. Bannister, E. Trasatti, P. Pasquiali, and S. Salvi (2012). The 2010-2011 Canterbury, New Zealand, seismic sequence: multiple source analysis from InSAR data and modelling. *Journal of Geophysical Research* 117, B08305, doi:10.1029/2012JB009178.
- Avery, H.R., J.B. Berrill, P.F. Coursey, B.L. Deam, M.B. Dewe, C.C. Francois, J.R. Pettinga, and M.D. Yetton (2004). The Canterbury University strong-motion recording project. Proceedings of 13th World Conference on Earthquake Engineering, Vancouver, British Columbia, 1-6 August 2004. *Canadian Association for Earthquake Engineering* paper no. 1335.
- Bannister, S., B. Fry, M. Reyners, J. Ristau, and H. Zhang (2011). Fine-scale relocation of aftershocks of the 22 February M_w 6.2 Christchurch earthquake using double-difference tomography. *Seismological Research Letters* 82, 839-845, doi:10.1785/gssrl.82.6.839.
- Beavan, J., M. Motagh, E. Fielding, N. Donnelly, and D. Collett (2012). Fault slip models of the 2010-2011 Canterbury, New Zealand, earthquakes from geodetic data, and observations of post-seismic ground deformation. *New Zealand Journal of Geology and Geophysics* 55, 207-221, doi:10.1080/00288306.2012.697472.
- Berryman, K.R., U.A. Cochran, K.J. Clark, G.P. Biasi, R.M. Langridge, and P. Villamor (2012). Major earthquakes occur regularly on an isolated plate boundary. *Science* 336, 1690-1693, doi:10.1126/science.1218959.

- Choy, G.L., J.L. Boatwright, and S. Kirby (2001). The radiated seismic energy and apparent stress of interplate and intraplate earthquakes at subduction zone environments: implications for seismic hazard estimate. *USGS Open-File Report* 01-005, 10 p.
- Cochran, E.S., J.F. Lawrence, C. Christensen, and R.S. Jakka (2009). The Quake-Catcher Network: citizen science expanding seismic horizons. *Seismological Research Letters* 80, 26-30.
- Cochran, E.S., J.F. Lawrence, A. Kaiser, B. Fry, A.I. Chung and C. Christensen (2011). Comparison between low-cost and traditional MEMS accelerometers: a case study from the *M* 7.1 Darfield, New Zealand, aftershock deployment. *Annals of Geophysics* 54, 728-737, doi:10.4401/ag-5268.
- Cooper, A.F., and R.J. Norris (1990). Estimates for timing of the last coseismic displacement on the Alpine fault, northern Fiordland, New Zealand. *New Zealand Journal of Geology and Geophysics* 33, 309-307.
- Cowan, H.A. (1991). The North Canterbury earthquake of September 1, 1888. *Bulletin of the New Zealand Society for Earthquake Engineering* 43, 222-227.
- Dorn, C., A.G. Green, R. Jongens, S. Carpentier, A.E. Kaiser, F. Campbell, H. Horstmeyer, J. Campbell, M. Finnemore, and J. Pettinga (2010). High-resolution seismic images of potentially seismogenic structures beneath the northwest Canterbury Plains, New Zealand. *Journal of Geophysical Research* 115, B11303, doi:10.1029/2010JB007459.
- Doser, D.I., T.H. Webb, and D.E. Maunder (1999). Source parameters of large historical (1918-1962) earthquakes, South Island, New Zealand. *Geophysical Journal International* 139, 769-794.
- Eberhart-Phillips, D., P.J. Haeussler, J.T. Freymueller, A.D. Frankel, C.M. Rubin, P. Craw, N.A. Ratchkovski, G. Anderson, G.A. Carver, A.J. Crone, T.E. Dawson, H. Fletcher, R. Hansen, E.L. Harp, R.A. Harris, D.P. Hill, S. Hreinsdottir, R.W. Jibson, L.M. Jones, R. Kayen, D.K. Keefer, C.F. Larsen, S.C. Moran, S.F. Personius, G. Plafker, B. Sherrod, K. Sieh, N. Sitar, and W.K. Wallace (2003). The 2002 Denali fault earthquake, Alaska: a large magnitude slip-partitioned event. *Science* 300, 1113-1118.
- Elliot, J.R., E.K. Neissen, P.C. England, J.A. Jackson, S. Lamb, Z. Li, M. Oehlers, and B. Parsons (2012). Slip in the 2010-2011 Canterbury earthquakes, New Zealand. *Journal of Geophysical Research* 117, B03401, doi:10.1029/2011jb008868.
- Forsyth, P.J., D.J.A. Barrell, and R. Jongens (2008). Geology of the Christchurch Area. Institute of Geological and Nuclear Sciences 1:250 000 geological map 16, 1 sheet + 67 pp. Lower Hutt, NZ: GNS Science.
- Fry, B., and M.C. Gerstenberger (2011). Large apparent stresses from the Canterbury earthquakes of 2010 and 2011. *Seismological Research Letters* 82, 833-838, doi:10.1785/gssrl.82.6.833.
- Fry, B., F.J. Davey, D. Eberhart-Phillips, and S. Lebedev (2014). Depth variable crustal anisotropy, patterns of crustal weakness, and destructive earthquakes in Canterbury, New Zealand. *Earth and Planetary Science Letters* 392, 50-57, doi:10.1016/j.epsl.2014.02.013.
- Gerstenberger, M., G. McVerry, D Rhoades, and M. Stirling (2014). Seismic hazard modelling for the recovery of Christchurch, New Zealand. *Earthquake Spectra* doi:10.1193/021913EQS037M.

- Gledhill, K., R., Robinson, R. Abercrombie, T. Webb, J. Beavan, J. Cousins, and D. Eberhart-Phillips (2000). The M_w 6.2 Cass, New Zealand earthquake of 24 November 1995: reverse faulting in a strike-slip regime. *New Zealand Journal of Geology and Geophysics* 43, 255-269.
- Gledhill, K., J. Ristau, M. Reyners, B. Fry, and C. Holden (2011). The Darfield (Canterbury, New Zealand) M_w 7.1 earthquake of September 2010: a preliminary seismological report. *Seismological Research Letters* 82, 378-386, doi:10.1785/gssrl.82.3.378.
- Hayes, G.P., R.W. Briggs, A. Sladen, E.J. Fielding, C. Prentice, K. Hudnut, P. Mann, F.W. Taylor, A.J. Crone, R. Gold, T. Ito, and M. Simons (2010). Complex rupture during the 12 January 2010 Haiti earthquake. *Nature Geoscience* 3, 800-805, doi:10.1038/NGEO977.
- Holden, C., and J. Beavan (2012). Kinematic source studies of the ongoing (2010-2011) sequence of recent large earthquakes in Canterbury. Paper 061 (8 p) *in* Implementing lessons learnt: 2012 Conference, 13-15 April, Christchurch, New Zealand, Christchurch: New Zealand Society for Earthquake Engineering.
- Lawrence, J.F., E.S. Cochran, A. Chung, A. Kaiser, C.M. Christensen, R. Allen, J.W. Baker, B. Fry, T. Heaton, D. Kilb, M.D. Kohler and M. Taufer (2014). Rapid earthquake characterization using MEMS accelerometers and volunteer hosts following the M 7.2 Darfield, New Zealand, earthquake. *Bulletin of the Seismological Society of America* 104, 184-192, doi:10.1785/0120120196.
- Petersen, T., K. Gledhill, M. Chadwick, N. Gale, and J. Ristau (2011). The New Zealand national seismograph network. *Seismological Research Letters* 82, 9-20, doi:10.1785/gssrl.82.1.9.
- Quigley, M., R. Van Dissen, P. Villamor, N. Litchfield, D. Barrell, K. Furlong, T. Stahl, B. Duffy, E. Bilderback, D. Noble, D. Townsend, J. Begg, R. Jongens, W. Ries, J. Claridge, A. Klahn, H. Mackenzie, A. Smith, S. Hornblow, R. Nicol, S. Cox, R. Langridge, and K. Pedley (2010). Surface rupture of the Greendale fault during the M_w 7.1 Darfield (Canterbury) earthquake, New Zealand: initial findings. *Bulletin of the New Zealand Society for Earthquake Engineering* 43, 236-242.
- Reyners, M., D. Eberhart-Phillips, and S. Martin (2013). Prolonged Canterbury earthquake sequence linked to widespread weakening of strong crust. *Nature Geoscience* 7, 34-37, doi:10.1038/NGEO2013.
- Rhoades, D.A., and R.J. Van Dissen (2003). Estimates of the time varying hazard of rupture of the Alpine fault, New Zealand, allowing for uncertainties. *New Zealand Journal of Geology and Geophysics* 46, 479-488.
- Ristau, J. (2011). Focal mechanism analysis of Christchurch boxing day aftershocks. GNS Science Consultancy Report 2011/43, 7 p.
- Sibson, R., F. Ghisetti, and J. Ristau (2011). Stress control of an evolving strike-slip fault system during the 2010-2011 Canterbury, New Zealand, earthquake sequence. *Seismological Research Letters* 82, 824-832, doi:10.1785/gssrl.82.6.824.
- Steady, S., A. Jiménez, and C. Holden (2014). Stress triggering and the Canterbury earthquake sequence. *Geophysical Journal International* 196, 473-480, doi:10.1093/gji/ggt380.
- Stirling, M., M. Gerstenberger, N. Litchfield, G. McVerry, W. Smith, J. Pettinga, and P. Barnes (2008). Seismic hazard of the Canterbury region, New Zealand: new earthquake source model and methodology. *Bulletin of the New Zealand Society for Earthquake Engineering* 41, 51-67.
-

Sutherland, R.D. *et al.* (2007). Do great earthquakes occur on the Alpine fault in central South Island, New Zealand?, *in* A Continental Plate Boundary: Tectonics at South Island, New Zealand, p. 235-251, eds. Okaya, D., Stern, T., and Davey, F., Geophysical Monograph 175, American Geophysical Union, Washington, DC.

Wessel, P., and W.H.F. Smith (1991). Free software helps map and display data. *EOS Transactions AGU* 71, 441.

Yetton, M.D., A. Wells, and N. Traylen (1998). The probability and consequences of the next Alpine fault earthquake, EQC Research Report 95/193,, New Zealand Earthquake Commission, Wellington, New Zealand.

Zhang, H., and Z. Ge (2010). Tracking the rupture of the 2008 Wenchuan earthquake by using the relative back-projection method. *Bulletin of the Seismological Society of America* 100, 2551-2560, doi:10.1785/0120090243.